4th MASHCON, Hamburg - Uliczka et al. (eds) - © 2016 Bundesanstalt für Wasserbau ISBN 978-3-939230-38-0 (Online)
DOI: 10.18451/978-3-939230-38-0_31

CAPTIVE MODEL TESTS BASED 6 DOF SHALLOW WATER MANOEUVRING MODEL

G Delefortrie, Flanders Hydraulics Research, Belgium
K Eloot, Flanders Hydraulics Research, Belgium and Ghent University, Belgium
E Lataire, Ghent University, Belgium
W Van Hoydonck, Flanders Hydraulics Research, Belgium
M Vantorre, Ghent University, Belgium

SUMMARY

This article presents the formulation of the 6 DOF manoeuvring model in calm water for ships with conventional propulsion and steering (1 fixed propeller, 1 stock rudder) as it is used on the ship manoeuvring simulators at Flanders Hydraulics Research (FHR). The coefficients are determined based on the results of captive model tests carried out in the Towing Tank for Manoeuvres in Shallow Water at FHR (co-operation with Ghent University). In this article the benchmark ship KVLCC2 is used as an example for discussion, based on the tests that were carried out at full draft and water depths of 180%, 130% and 120% of the draft. Fast time simulations have been carried out based on the developed manoeuvring model and the trajectories in 6 DOF are compared with the SIMMAN 2014 benchmark manoeuvres.

NOMENCLATURE

a_H	parameter (-)
A_R	rudder area (m²)
A_W	waterline area (m²)
B	breadth (m)
C_B	block coefficient (-)
C_D	drag coefficient (-)
C_L	lift coefficient (-)
C_Q	torque coefficient (-)
C_T	thrust coefficient (-)
D_P	propeller diameter (m)
F_N	force, perpendicular on the rudder (N)
Fr_h	water depth based Froude number (-)
F_X	longitudinal rudder force (N)
F_Y	lateral rudder force (N)
g	gravity acceleration (m/s²)
$\overline{GM}_T$	initial transverse stability lever (m)
$\overline{GM}_L$	initial longitudinal stability lever (m)
h	water depth (m)
$\bar{I}$	inertia tensor (kgm²)
I_{**}	moment or product of inertia (kgm²)
K	roll moment (Nm)
$\overline{KM}_T$	transverse metacentric height (m)
$\overline{KM}_L$	longitudinal metacentric height (m)
k	~ distance propeller – rudder (-)
L	length (m)
M	pitch moment (Nm)
m	ship's mass (kg)
N	yaw moment (Nm)
n	propeller rate (1/s)
p	roll velocity (rad/s)
q	pitch velocity (rad/s)
Q_P	propeller shaft torque (Nm)
r	yaw velocity (rad/s)
T	draft (m)
t	time (s); thrust deduction factor (-)
T_P	propeller thrust (N)
Tu_h	Tuck parameter, eq. 27 (-)
u	longitudinal ship velocity (m/s)
u_R	longitudinal velocity near rudder (m/s)
ukc	under keel clearance
V	total ship velocity (m/s)
v	lateral ship velocity (m/s)
v_R	lateral velocity near rudder (m/s)
w	vertical ship velocity (m/s)
w_R	wake factor for the rudder (-)
w_T	wake factor for the thrust (-)
X	longitudinal force (N)
x	longitudinal coordinate (m)
$\overline{\boldsymbol{x}}_{\boldsymbol{G}}$	position of centre of gravity (m)
x_G	longitudinal centre of gravity (m)
x_H	parameter (-)
x_R	longitudinal position of rudder (m)
Y	sway force (N)
y	lateral coordinate (m)
y_G	lateral centre of gravity (m)
Z	heave force (N)
z_G	vertical centre of gravity (m)
z_H	parameter (-)
z_{HX}	parameter (-)
z_R	vertical position rudder centreline (m)
α	inflow angle (deg)
β	drift angle (deg)
β_R	drift angle near rudder (deg)
γ	yaw angle (deg)
γ^*	propeller loading angle for yaw (deg)
Δ	displacement (N)
δ	rudder angle (deg)
δ_0	rudder asymmetry correction (deg)
$\varepsilon^{(*)}$	(apparent) propeller loading angle (deg)
η	propeller diameter ÷ rudder height (-)
θ	pitch angle (deg)
ξ	parameter (-)
ρ	water density (kg/m³)
φ	heel angle (deg)
φ^*	propeller loading angle for sway (deg)
φ_*	phase angle (deg)
χ	yaw-drift correlation angle (deg)

Subscripts

0	tank fixed
IC	inertial and centrifugal
H	hull
hyd	hydrostatic
OA	over all
P	propeller
PP	between perpendiculars
R	rudder
ret	retardation

Superscripts

.	time derivative
n	propeller dependent

1 INTRODUCTION

Mathematical manoeuvring models commonly focus on the prediction of the longitudinal force, sway force and yawing moment acting on the ship to predict her path in the horizontal plane. At Flanders Hydraulics Research (FHR), manoeuvring models with three degrees of freedom (3 DOF) have been applied successfully to study the ship's manoeuvring behaviour in different shallow water areas. This manoeuvring model was presented in [1].

In 2009 the roll motion was added as a fourth degree of freedom, specifically to include the roll motion for inland ships in the, at that time, newly built inland navigation simulator Lara. Since then the roll motion has been studied for seagoing vessels as well due to the interaction of the roll motion with the other degrees of freedom.

The sinkage and trim of the vessel were mostly treated separately from the measured forces. This is mainly due to the setup of the tests in the Towing Tank for Manoeuvres in Shallow Water at FHR [2] (co-operation with Ghent University) where the ship models are always free to heave and pitch. As such the sinkage and trim were only occasionally added to the simulation models through kinematic squat mathematical models. However, since the IMO issued the Energy Efficiency Design Index with specific regulations considering the manoeuvring behaviour in wind and waves, the research in this topic has received a growing interest.

To cope with the manoeuvring behaviour in waves and give attention to all degrees of freedom, a 6 DOF manoeuvring model is compulsory. Even in calm shallow water conditions a 6 DOF manoeuvring model offers advantages, such as the inclusion of squat and assessment of the dynamic under keel clearance. As a stepping stone towards a full 6 DOF model to cope with manoeuvring in waves, a 6 DOF manoeuvring model in calm water has been under development since 2012.

In this article this mathematical model will be presented, applied to the benchmark ship KVLCC2 [6]. The mathematical model is based mainly on the outcome of captive manoeuvring tests carried out in the towing tank of FHR. Some simulations are presented as well, which compare the free running model tests carried out with the KVLCC2 in the frame of SIMMAN2014, as such this research is a follow up of [3,4].

2 EXPERIMENTAL PROGRAM

2.1 KVLCC2

The KVLCC2 is a benchmark ship developed at KRISO in Korea. FHR possesses a 1/75 scale model of this ship, called T0Z. The full scale particulars are presented in Table 1. The mass distributions of the ship model during captive and free running tests can be found in Tables 2 and 3.

Table 1. Ship data of T0Z at tested draft (even keel)

KVLCC2 (T0Z) – single propeller – single rudder			
L_{OA} (m)	325.0	#propeller blades	4
L_{PP} (m)	320.0	D_P (m)	9.86
B (m)	58.0	$P/_D$ (-)	0.721
T (m)	20.8	AEP (-)	0.431
C_B (-)	0.810	A_R (m²)	111.7
m (kg)	3.130 10^8	Model scale	1:75
$\overline{KM}_T$ (m)	24.29	$\overline{KM}_L$ (m)	398.5

Table 2. Loading condition during captive model tests (model scale)

$$\overline{\boldsymbol{x}}_{\boldsymbol{G}} = \begin{bmatrix} 0.151 \pm 0.002 \\ 0 \\ 0.0 \pm 0.003 \end{bmatrix} m;$$

$$\bar{\boldsymbol{I}} = \begin{bmatrix} 42.9 \pm 2 & 0 & NA \\ 0 & 837.2 \pm 2 & 0 \\ NA & 0 & 867.2 \pm 2 \end{bmatrix} kgm^2$$

Table 3. Loading condition during free running model tests (model scale)

$$\overline{\boldsymbol{x}}_{\boldsymbol{G}} = \begin{bmatrix} 0.149 \pm 0.002 \\ 0 \\ 0.012 \pm 0.003 \end{bmatrix} m;$$

$$\bar{\boldsymbol{I}} = \begin{bmatrix} 49.4 \pm 2 & 0 & NA \\ 0 & 839.6 \pm 2 & 0 \\ NA & 0 & 877.5 \pm 2 \end{bmatrix} kgm^2$$

2.2 CAPTIVE MODEL TESTS

The captive model tests were carried out in 2012 and 2015 in the towing tank at FHR at three different under keel clearances, see Table 4.

Table 4. Tested under keel clearances (captive mode)

Environment	ukc	Execution date
T0Z06A01	80%	August 2012
T0Z09A01	30%	March 2015
T0Z06A03	20%	September 2012

For each under keel clearance about 300 tests have been carried out. The speeds were varied between -3.5 knots and 15.5 knots. A large range of kinematic and control parameters was covered to be able to simulate four quadrant harbour manoeuvres. Both drift and yaw angle were varied over 360 deg. Rudder angles between hard port and hard starboard (±35 deflection angles) were combined with propeller rates between harbour full ahead and astern.

The experimental programme consisted of:

- bollard pull tests;
- stationary tests;
- harmonic sway tests;
- harmonic yaw tests;
- multimodal tests with variable speed, rudder angle and/or propeller rate.

The following data were measured:

- longitudinal force;
- lateral force components fore and aft;
- roll moment;
- vertical motion (4 measuring posts: fore/aft, port/starboard);
- rudder parameters (normal and tangential forces, torque, angle);
- propeller parameters (torque, thrust, rpm).

The coefficients of the mathematical model have been determined for each ukc. For an arbitrary ukc the hydrodynamic forces are linearly interpolated between the calculated forces from the available mathematical models.

2.3 FREE RUNNING MODEL TESTS

In 2010 free running model tests were carried out for SIMMAN2014. In this article all the repetitions of the free running model tests carried out at an ukc of 20% will be used as a basis for comparison. The approach speed was always according to 7 knots full scale. The following tests have been carried out:

- 10/2.5 zigzag test, both starting to port and to starboard;
- 20/5 zigzag test, both starting to port and to starboard;
- Partial turning circle at 35 deg rudder deflection, both starting to port and to starboard.

The following data were measured:

- ship position in the horizontal plane;
- vertical motion (3 measuring posts to cover heave, roll and pitch);
- rudder parameters (normal and tangential forces, torque, angle);
- propeller parameters (torque, thrust, rpm).

3 DYNAMICS IN 6 DOF

3.1 COORDINATE SYSTEM

Figure 1 shows the used horizontal bound right handed coordinate system for a regular ship in 6 degrees of freedom. The shown coordinate systems are the tank-fixed ($O_0x_0y_0z_0$), the ship-fixed ($Oxyz$) and the ship-fixed horizontal bound ($Ox'y'z'$) coordinate systems. The expected vertical motions during calm water manoeuvring are small, so that the ship fixed system can be considered equal to the horizontal bound.

The origin O of the ship fixed system is determined as follows:

- located amidships;
- on the static waterline corresponding to the static loading condition;
- in the longitudinal plane of symmetry of the ship.

As a consequence the moments of centrifugal terms and other inertia forces must be taken into account.

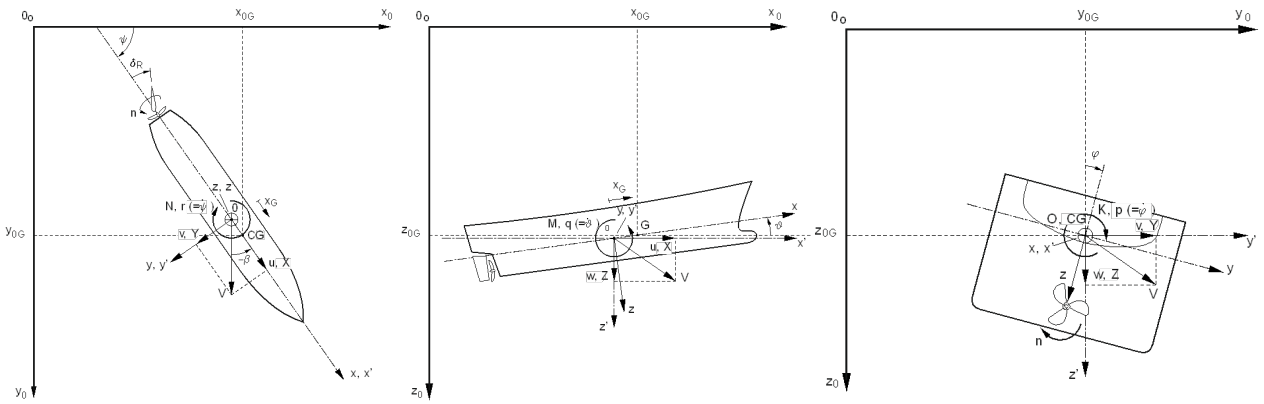

Figure 1. Ship and earth fixed coordinate systems in 6 degrees of freedom: projections on the x_0y_0-plane, y_0z_0-plane and z_0x_0-plane.

3.2 ASSUMPTIONS

Apart from the assumption that the ship fixed coordinate system is horizontal bound, additional assumptions are needed.

The vessel is always free to heave and pitch, but for simulation purposes, the pitch moment and the heave force are needed for formulating the corresponding equations of motion. It is assumed that the mean sinkage and the trim can be considered solely the result of the counteracting hydrostatic heave force Z and the counteracting pitch moment M. The displacement of the ship and the counteracting buoyancy force are left out of the equations (the heave force is the disturbance force). In reality the squat of the vessel is caused by the hydrodynamic equilibrium with the free surface deformation around the ship and not by an external heave or pitch moment.

Due to the limitations of the towing tank carriage, which only enables steering in the horizontal plane, the presented 6 DOF manoeuvring model is to be considered a 3+3 DOF model where only the horizontal motions are fully coupled with the forces and moments in 6 degrees. The effect of vertical motions are either implicitly covered, found by other means or simply neglected.

3.3 FORMULATION

3.3 (a) Inertia and centrifugal terms

Because the KVLCC2 possesses a longitudinal plane of symmetry ($y_G = 0$) the following set of equations, expressed in the ship bound axis system, may be used:

$$X = m[\dot{u} - vr + wq - x_G(q^2 + r^2) + z_G(\dot{q} + pr)] \quad (1)$$

$$Y = m[\dot{v} + ur - wp + x_G(\dot{r} + pq) + z_G(-\dot{p} + qr)] \quad (2)$$

$$Z = m[\dot{w} + uq - vp + x_G(-\dot{q} + pr) - z_G(p^2 + q^2)] \quad (3)$$

$$K = (I_{xx}\dot{p} - I_{xz}\dot{r}) - I_{xz}pq + \left(I_{zz} - I_{yy}\right)qr - m(\dot{v} + ur - wp)z_G \quad (4)$$

$$M = I_{yy}\dot{q} + (I_{xx} - I_{zz})pr + I_{xz}(p^2 - r^2) + m[-(\dot{w} + vp - uq)x_G + (\dot{u} - vr + wq)z_G] \quad (5)$$

$$N = (-I_{xz}\dot{p} + I_{zz}\dot{r}) + I_{xz}qr + \left(I_{yy} - I_{xx}\right)pq + m(\dot{v} + ur - wp)x_G \quad (6)$$

The inertia (acceleration dependent) and centrifugal (speed dependent) terms are supposedly included with the hull forces. Adding the effect of the hydrodynamic inertia terms to be modelled, leads to the reordered equations (7) – (12).

$$X_{IC} = (X_{\dot{u}} - m)\dot{u} + \left(X_{\dot{q}} - mz_G\right)\dot{q} + m(vr - wq) + mx_G(r^2 + q^2) - mz_G pr \quad (7)$$

$$Y_{IC} = (Y_{\dot{v}} - m)\dot{v} + \left(Y_{\dot{p}} + mz_G\right)\dot{p} + (Y_{\dot{r}} - mx_G)\dot{r} + m(wp - ur) - mx_G pq - mz_G qr \quad (8)$$

$$Z_{IC} = (Z_{\dot{w}} - m)\dot{w} + \left(Z_{\dot{q}} + mx_G\right)\dot{q} + m(vp - uq) - mx_G pr + mz_G(p^2 + q^2) \quad (9)$$

$$K_{IC} = (K_{\dot{v}} + mz_G)\dot{v} + \left(K_{\dot{p}} - I_{xx}\right)\dot{p} + (K_{\dot{r}} + I_{xz})\dot{r} + I_{xz}pq - \left(I_{zz} - I_{yy}\right)qr + mz_G(ur - wp) \quad (10)$$

$$M_{IC} = (M_{\dot{u}} - mz_G)\dot{u} + (M_{\dot{w}} + mx_G)\dot{w} + \left(M_{\dot{q}} - I_{yy}\right)\dot{q} - (I_{xx} - I_{zz})pr - I_{xz}(p^2 - r^2) + mx_G(vp - uq) - mz_G(wq - vr) \quad (11)$$

$$N_{IC} = (N_{\dot{v}} - mx_G)\dot{v} + \left(N_{\dot{p}} + I_{xz}\right)\dot{p} + (N_{\dot{r}} - I_{zz})\dot{r} - I_{xz}qr - \left(I_{yy} - I_{xx}\right)pq - mx_G(ur - wp) \quad (12)$$

The blue parameters are mostly found with a regression analysis based on the captive towing tank measurements. Due to the horizontal 3 DOF nature of the carriage, these parameters have to be found by other means:

- $Z_{\dot{w}}, Z_{\dot{q}}, M_{\dot{w}}, M_{\dot{q}}$ have to be computed numerically, although the available software is mostly not accurate enough in shallow water. Alternatively they can be determined based on labour intensive pitch and heave decay tests. They are only determined for the natural frequency.
- $K_{\dot{p}}$ is found after execution of roll decay tests.
- The grey values are unknown, but are supposed to be rather small and therefore neglected. For instance I_{xz} has a magnitude of 1 kgm² on model scale (but was not determined for the KVLCC2, *NA* in Table 2 and 3). At present they are simply neglected in the simulator.

The left hand side of equations (1) – (6) are the sum of external forces (e.g. wind, tugs,…, not considered in this article), the speed-dependent hydrodynamic forces, the control forces and the hydrostatic terms. The speed-dependent behaviour (hydrodynamic damping) is considered together with some retardation terms, hydrostatic terms, inertia and centrifugal terms as hull forces. The modelling of these will be tackled in section 4. The modelling of the control forces is dealt with in sections 5 and 6.

3.3 (b) Retardation terms

The ship's squat shows retardation during acceleration of the ship model. Until now this retardation is modelled using equations (13) – (14).

$$Z_{ret} = Z_{\dot{u}}\dot{u} + Z_{\dot{v}}|\dot{v}| + Z_{\dot{r}}|\dot{r}| \quad (13)$$

$$M_{ret} = M_{\dot{v}}|\dot{v}| + M_{\dot{r}}|\dot{r}| \quad (14)$$

It should be emphasized that the present formulation is a pragmatic one, but leaves room for improvement, as it could have undesirable results during the simulation process. The other degrees of freedom do not include retardation. $M_{\dot{u}}$ is already included in equation (11) but is expected to have implicit retardation.

3.3 (c) Hydrostatic terms

In the vertical degrees of freedom hydrostatic equilibrium is achieved with the following equations:

$$Z_{hyd} = -\frac{\partial \Delta}{\partial T} dT \approx -\rho g A_W z \quad (15)$$

$$K_{hyd} = -\Delta \overline{GM}_T \varphi \quad (16)$$

$$M_{hyd} = -\Delta \overline{GM}_L \theta \quad (17)$$

The use of (constant) $\overline{GM}_T$ and $\overline{GM}_L$ is acceptable due to the assumption of small vertical movement in calm water.

4 MATHEMATICAL MODEL: HULL FORCES

4.1 OVERVIEW

The hull forces are expressed according to equations (18) – (23).

$$X_H = X_{IC} + \frac{1}{2}\rho LT(u^2+v^2)X'^{(\beta)} + \frac{1}{2}\rho LT\left(u^2+\left(\frac{1}{2}rL\right)^2\right)X'^{(\gamma)} + \frac{1}{2}\rho LT\left(v^2+\left(\frac{1}{2}rL\right)^2\right)X'^{(\chi)} \quad (18)$$

$$Y_H = Y_{IC} + \frac{1}{2}\rho LT(u^2+v^2)Y'^{(\beta)} + \frac{1}{2}\rho LT\left(u^2+\left(\frac{1}{2}rL\right)^2\right)Y'^{(\gamma)} + \frac{1}{2}\rho LT\left(v^2+\left(\frac{1}{2}rL\right)^2\right)Y'^{(\chi)} \quad (19)$$

$$Z_H = Z_{IC} + Z_{ret} + Z_{hyd} + \Delta T u_h Z'^{(\beta)} + \frac{1}{2}\rho LT\left(u^2+\left(\frac{1}{2}rL\right)^2\right)Z'^{(\gamma)} + \frac{1}{2}\rho LT\left(v^2+\left(\frac{1}{2}rL\right)^2\right)Z'^{(\chi)} + Z_w w + Z_q q \quad (20)$$

$$K_H = K_{IC} + K_{hyd} + \frac{1}{2}\rho LT^2(u^2+v^2)K'^{(\beta)} + \frac{1}{2}\rho LT^2\left(u^2+\left(\frac{1}{2}rL\right)^2\right)K'^{(\gamma)} + \frac{1}{2}\rho LT^2\left(v^2+\left(\frac{1}{2}rL\right)^2\right)K'^{(\chi)} + \left[K_p - |\varphi|\sqrt{\Delta \overline{GM}_T\left((-K_{\dot{p}} + I_{xx})\right)}\right]p + K_{up}up \quad (21)$$

$$M_H = M_{IC} + M_{ret} + M_{hyd} + \Delta LT u_h M'^{(\beta)} + \frac{1}{2}\rho L^2 T\left(u^2+\left(\frac{1}{2}rL\right)^2\right)M'^{(\gamma)} + \frac{1}{2}\rho L^2 T\left(v^2+\left(\frac{1}{2}rL\right)^2\right)M'^{(\chi)} + M_w w + M_q q \quad (22)$$

$$N_H = N_{IC} + \frac{1}{2}\rho L^2 T(u^2+v^2)N'^{(\beta)} + \frac{1}{2}\rho L^2 T\left(u^2+\left(\frac{1}{2}rL\right)^2\right)N'^{(\gamma)} + \frac{1}{2}\rho L^2 T\left(v^2+\left(\frac{1}{2}rL\right)^2\right)N'^{(\chi)} \quad (23)$$

In the above equations the following parameters have been introduced:

- The hydrodynamic angles (horizontal speed combinations):

  $$\beta = \arctan\left(\frac{-v}{u}\right) \quad (24)$$

  $$\gamma = \arctan\left(\frac{0.5rL}{u}\right) \quad (25)$$

  $$\chi = \arctan\left(\frac{0.5rL}{v}\right) \quad (26)$$

  respectively referred to as drift, yaw and drift-yaw correlation angle. The range of the arctan function is extended to [-π,π] for four quadrants.
- The Tuck parameter [5]:

  $$Tu_h = \frac{Fr_h}{\sqrt{1-Fr_h^2}} \quad (27)$$

  expressed as a function of the depth-related Froude number:

  $$Fr_h = \frac{V}{\sqrt{gh}} \quad (28)$$

The blue terms in equations (18) – (23) need to be modelled. The way this is performed depends on the term:

- The effect of the hydrodynamic angles is based on the results of the captive manoeuvring tests. The influence is modelled in a tabular way, meaning that a function is built with discrete values for a selection of angles β, γ and χ. In between two values a linear interpolation is applied. The results of the regression are highly dependent on a good selection of the discrete values. They should correspond with values obtained during the captive model tests.
- The vertical speed dependencies can be obtained as follows:
  - K_p, K_{up} are determined based on roll decay tests, performed at different forward speeds.
  - Z_w, Z_q, M_w, M_q have to be computed using a similar method as for the corresponding acceleration dependent derivatives.

Within this article it is impossible to discuss every expression in detail. In the following paragraphs some examples of drift and yaw functions will be given.

4.2 DRIFT FORCES

Figure 2 shows the influence of the ship's drift angle on the force components in 6 DOF. The drift force is to be considered as the main force component, i.e. at zero drift, yaw and yaw-drift correlation angle, the entire force component is considered as a drift force.

For all DOFs, except roll, an increasing trend is observed for decreasing under keel clearance. Pure sway motion mainly affects the sway and heave forces and the roll moment. The other degrees of freedom are affected when surge and sway velocity are of the same magnitude.
Clear symmetry patterns can be observed in the different functions, however perfect symmetry is not achieved due to imperfections of the hull, carriage, modelling… Prior to simulations the functions are made (anti-)symmetric.

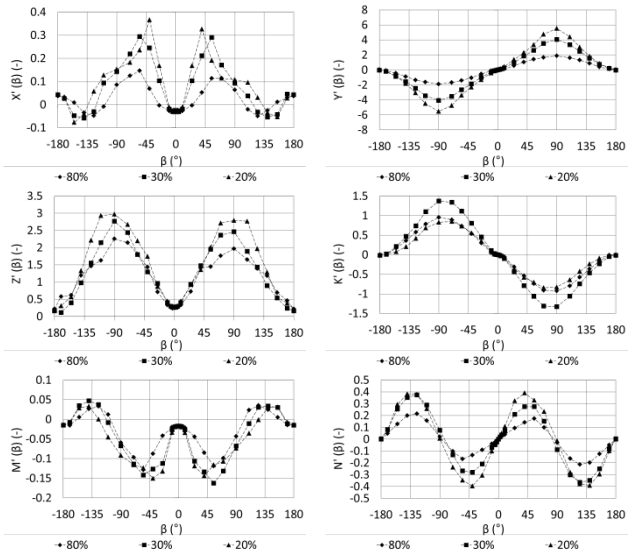

Figure 2. Drift functions in 6 DOF for the tested under keel clearances.

4.3 YAW FORCES

The influence of the yaw angle on the 6 DOF force components is shown in Figure 3. Increasing the yaw rate and decreasing the under keel clearance will increase the magnitude of the force or moment. As for the drift force, symmetry patterns are clearly visible.

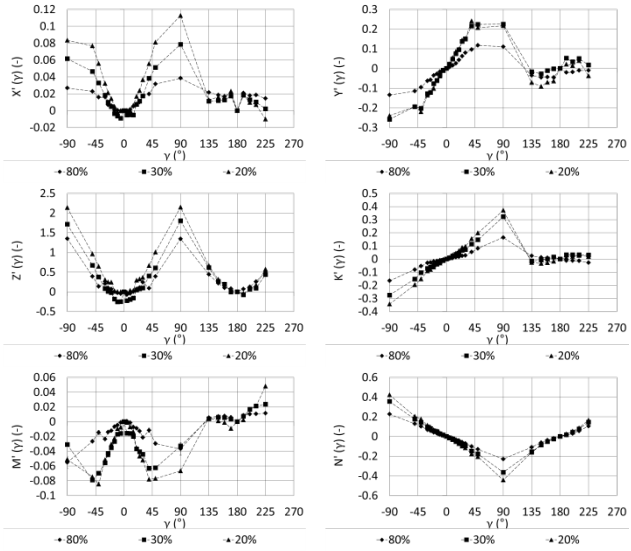

Figure 3. Yaw functions in 6 DOF for the tested under keel clearances.

5 MATHEMATICAL MODEL: PROPULSION FORCES

5.1 PROPELLER THRUST AND TORQUE

The propeller thrust is modelled by determining the wake factor in:

$$\varepsilon = \arctan\left(\frac{(1-w_T)u}{0.7\pi n D_P}\right) \tag{29}$$

So that the thrust can be predicted as follows:

$$T_P = \frac{0.7^2}{8}\pi^3 \rho n^2 D_P^4 C_T(\varepsilon)(1+\tan^2\varepsilon) \tag{30}$$

in which C_T is an alternative formulation of K_T to allow for four quadrant operations:

- Quadrant 1: $u \geq 0; n \geq 0$
- Quadrant 2: $u \geq 0; n < 0$
- Quadrant 3: $u < 0; n \leq 0$
- Quadrant 4: $u < 0; n > 0$

The propeller thrust in open water was determined and it is found to be comparable to the open water characteristic of the HMRI model available on the SIMMAN2014 website [6]. Analogously, the propeller shaft torque is modelled using the expression:

$$Q_P = \frac{0.7^2}{8}\pi^3 \rho n^2 D_P^5 C_Q(\varepsilon)(1+\tan^2\varepsilon) \tag{31}$$

In most cases a slightly different wake factor is needed for the propeller shaft torque. Both wake factors are expressed as a function of the apparent propeller loading,

$$\varepsilon^* = \arctan\left(\frac{u}{0.7\pi n D_P}\right) \tag{32}$$

see Figure 4, for the first quadrant. The model self-propulsion point during simulations is $\varepsilon^* \approx 12°$. In the other quadrants the wake factor equals zero, however, between the first and the fourth quadrant a smooth transition is needed.

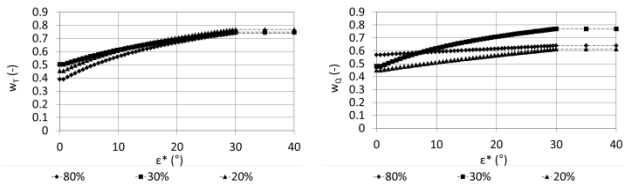

Figure 4. Wake factors for the propeller thrust (T) and shaft torque (Q).

5.2 PROPELLER INDUCED FORCES

5.2 (a) Longitudinal force

The propulsion induced longitudinal force is modelled with a thrust deduction factor:

$$X_P = \left(1 - t(\varepsilon^*, \varphi^*, \gamma^*)\right) T_P \tag{33}$$

which depends on different propeller loading angles:

$$\varphi^* = \arctan\left(\frac{|v|}{0.7\pi n D_P}\right) \tag{34}$$

$$\gamma^* = \arctan\left(\frac{|0.5rL|}{0.7\pi n D_P}\right) \tag{35}$$

as follows:

$$t = f(\varepsilon^*) + q_1(\varepsilon^*)\varphi^*\xi_1 + q_3(\varepsilon^*)\varphi^*\xi_3 + q_4(\varepsilon^*)\gamma^*\xi_4 \tag{36}$$

$q_j(\varepsilon^*)$ is equal to 1 in quadrant j and equal to zero in the other quadrants.

Figure 5 shows the thrust deduction in the first quadrant near the model self-propulsion point. Thrust deduction increases with decreasing propeller loading and with decreasing water depth (80% versus 20-30 % ukc), but for bollard pull the opposite seems true.

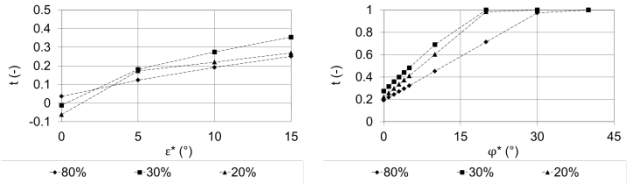

Figure 5. Thrust deduction factors close to the model self propulsion point.

5.2 (b) Forces in other DOF

The propeller induced forces in the other degrees of freedom are expressed using equations (37) – (41). The effect can be split in three parts:

- the propeller action affects the hydrodynamic inertia derivatives;
- a constant force or moment is observed, which depends on the thrust, yaw and drift angle;
- in the even quadrants, oscillations occur. The characteristics of these oscillations depend on the propeller loading.

In equations (37) – (41) the following parameters appear:

- K_1 equals the ship length based Froude number in the first quadrant and is 1 in the other quadrants;
- K_2 depends on the degree of oscillation, based on the yaw rate [1];
- K_3 equals the Tuck parameter (27) in the first quadrant and is 1 in the other quadrants.

In [7] the propulsion effect on squat has been modelled using an additional speed V_T which is a function of the propeller thrust T_P. To be more compliant with the mathematical models for the other degrees of freedom new equations are proposed. In contrast with the current work, the squat model in [7] accounted for the confinement of the waterway, but did not consider other quadrants than the first one.

As an example, Figure 6 shows the mean propeller induced forces and moments, while the amplitude of the oscillations are shown in Figure 7 for the second quadrant.

The propeller action mostly increases with decreasing under keel clearance and increasing yaw or drift angle. The oscillations are more pronounced in shallow water conditions.

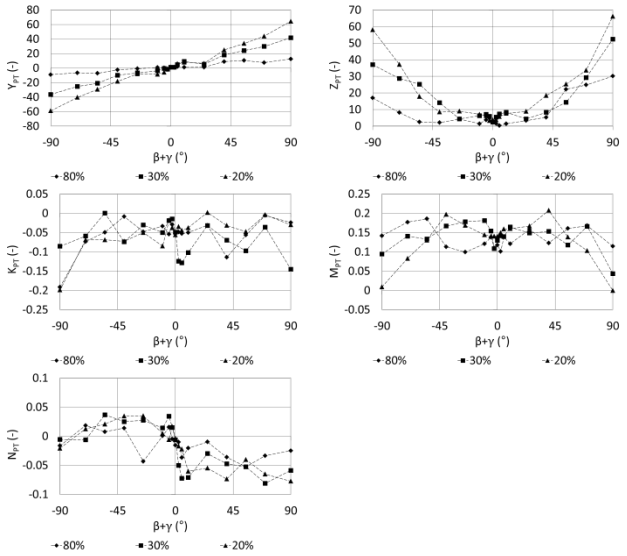

Figure 6. Mean propeller induced forces and moments in the first quadrant

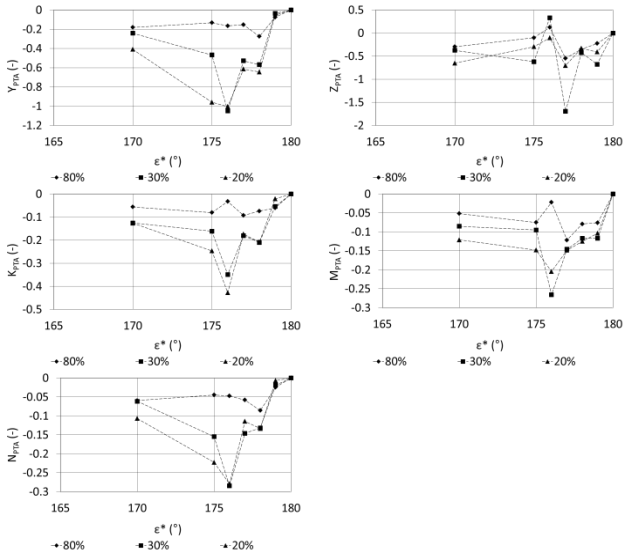

Figure 7. Amplitude of the propeller induced forces and moments in the second quadrant

$$Y_P = \left|\frac{n}{n_{MAX}}\right| [Y_{\dot{v}}^n \dot{v} + Y_{\dot{r}}^n \dot{r}] + \left[K_1[Y_{PT}(\beta, \varepsilon^*) + Y_{PT}(\gamma, \varepsilon^*)] + K_2 Y_{PTA}(\varepsilon^*) \cos\left(\omega(\varepsilon^*)t + \varphi_Y(\varepsilon^*)\right)\right] T_P(\varepsilon^*) \quad (37)$$

$$Z_P = \left[K_3[Z_{PT}(\beta, \varepsilon^*) + Z_{PT}(\gamma, \varepsilon^*)] + K_2 Z_{PTA}(\varepsilon^*) \cos\left(\omega(\varepsilon^*)t + \varphi_z(\varepsilon^*)\right)\right] T_P(\varepsilon^*) \quad (38)$$

$$K_P = \left|\frac{n}{n_{MAX}}\right| [K_{\dot{v}}^n \dot{v} + K_{\dot{r}}^n \dot{r}] + \left[[K_{PT}(\beta, \varepsilon^*) + K_{PT}(\gamma, \varepsilon^*)] + K_2 K_{PTA}(\varepsilon^*) \cos\left(\omega(\varepsilon^*)t + \varphi_K(\varepsilon^*)\right)\right] TT_P(\varepsilon^*) \quad (39)$$

$$M_P = \left[M_{PT}(\beta, \varepsilon^*) + M_{PT}(\gamma, \varepsilon^*) + K_2 M_{PTA}(\varepsilon^*) \cos\left(\omega(\varepsilon^*)t + \varphi_M(\varepsilon^*)\right)\right] LT_P(\varepsilon^*) \quad (40)$$

$$N_P = \left|\frac{n}{n_{MAX}}\right| [N_{\dot{v}}^n \dot{v} + N_{\dot{r}}^n \dot{r}] + \left[[N_{PT}(\beta, \varepsilon^*) + N_{PT}(\gamma, \varepsilon^*)] + K_2 N_{PTA}(\varepsilon^*) \cos\left(\omega(\varepsilon^*)t + \varphi_N(\varepsilon^*)\right)\right] LT_P(\varepsilon^*) \quad (41)$$

6 MATHEMATICAL MODEL: STEERING FORCES

6.1 FORCES ACTING ON THE RUDDER

6.1 (a) Formulation

Similar to the propeller thrust, the forces acting on the rudder are based on a model of the wake factor. To determine the open water lift and drag coefficients of the rudder, tests have been carried out with solely the rudder for a variety of inflow angles α (Fig.8).

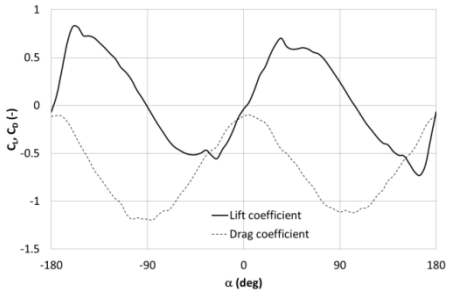

Figure 8. Measured lift and drag on the rudder of the KVLCC2 in open water.

When the rudder is behind the ship the inflow is affected, which is modelled with the effective rudder angle and drift near the rudder:

$$\alpha = \delta + \delta_0 + \beta_R \quad (42)$$

δ_0 (the rudder angle where the normal force F_N acting on the rudder becomes zero) is an offset for flow asymmetry:

$$\delta_0 = -\delta(F_N = 0) \quad (43)$$

β_R is the local drift angle at the rudder:

$$\beta_R = \arctan\left(\frac{-v_R}{u_R}\right) \quad (44)$$

u_R, v_R being the longitudinal and transverse component of the flow velocity near the rudder:

$$V_R = \sqrt{u_R^2 + v_R^2} \quad (45)$$

This way the forces on the rudder can be expressed as:

$$F_X = \frac{1}{2}\rho A_R V_R^2 [C_L \sin\beta_R + C_D \cos\beta_R] \quad (46)$$

$$F_Y = \frac{1}{2}\rho A_R V_R^2 [C_L \cos\beta_R - C_D \sin\beta_R] \quad (47)$$

6.1 (b) Modelling the inflow speed to the rudder

The problem is then to predict the velocity components near the rudder. The lateral component is assumed to be:

$$v_R = v + r x_R \quad (48)$$

The longitudinal component of the inflow speed is affected by both the propeller action and the hull. The formulation is based on impulse theory, which results in expression (52) for the first quadrant.

For the fourth quadrant the inflow is more complex due to the opposite flow generated by ship and propeller. The following methodology is used:

- Step 1: resolve the following implicit equations to determine the dominant flow component:

$$A = 0 \Leftrightarrow \sin\varepsilon = -k\sqrt{\frac{|C_T|}{\left(1+2k+\sqrt{\frac{1-\eta}{\eta}}\right)\left(1+\sqrt{\frac{1-\eta}{\eta}}\right)}} \quad (49)$$

$$B = 0 \Leftrightarrow \sin\varepsilon = -k\sqrt{\frac{|C_T|}{\left(1+2k-\sqrt{\frac{1-\eta}{\eta}}\right)\left(1-\sqrt{\frac{1-\eta}{\eta}}\right)}} \quad (50)$$

- Step 2:
  - if the propeller loading ε is smaller than B then the inflow velocity is determined by equation (53) and $\mathrm{sgn}(u_{RP})$ is negative;
  - if the propeller loading ε is larger than A then the inflow velocity is determined by the average of equations (53) and (54) with $\mathrm{sgn}(u_{RP})$ positive;
  - for intermediate points a linear interpolation, based on the propeller rate, is applied between the inflow velocity at point A and the inflow velocity at point B.

In the second and the third quadrant the forces acting on the rudder are rather small and the following simple expression for the inflow velocity is used:

$$u_R = \xi n + (1 - w_R)u \quad (51)$$

$$u_R = \frac{1-w_R}{1-w_T}\sqrt{\left\{\eta\left[(1-k)\sin\varepsilon + k\sqrt{C_T + \sin^2\varepsilon}\right]^2 + (1-\eta)\sin^2\varepsilon\right\}\{[(1-w_T)u]^2 + [0.7\pi n D_P]^2\}} \quad (52)$$

$$u_R = \frac{1-w_R}{1-w_T}sgn(u_{RP})\sqrt{\left\{\eta\left[(1+k)\sin\varepsilon + k\sqrt{|C_T| + \sin^2\varepsilon}\right]^2 - sgn(u_{RP})(1-\eta)\sin^2\varepsilon\right\}\{[(1-w_T)u]^2 + [0.7\pi n D_P]^2\}} \quad (53)$$

$$u_R = \frac{1-w_R}{1-w_T}sgn(u_{RP})\sqrt{\left\{\eta\left[(1-k)\sin\varepsilon + k\sqrt{|C_T| + \sin^2\varepsilon}\right]^2 - sgn(u_{RP})(1-\eta)\sin^2\varepsilon\right\}\{[(1-w_T)u]^2 + [0.7\pi n D_P]^2\}} \quad (54)$$

The wake factor w_R in the above equations can be expressed as a tabular function of the rudder angle. A different function is necessary for the longitudinal and the lateral rudder force. As can be seen on Figure 9 the wake factor is also affected by the under keel clearance.

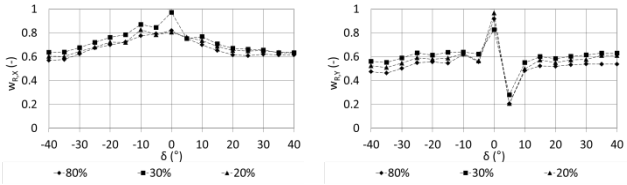

Figure 9. Wake factors for longitudinal (X) and lateral (Y) rudder force.

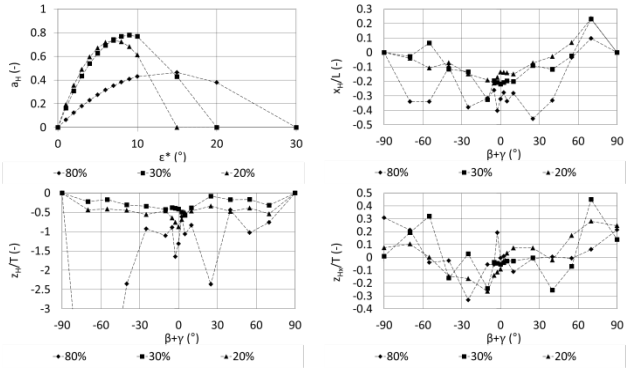

Figure 10. Rudder induced correlation coefficients for the first quadrant.

6.2 STEERING INDUCED FORCES

Once the hull and propeller induced forces are computed the remainder of the measured forces is used to compute the rudder induced part with the following equations:

$$X_R = F_X \quad (55)$$

$$Y_R = \left(1 + a_H(\varepsilon^*, \beta)\right)F_Y \quad (56)$$

$$Z_R = 0 \quad (57)$$

$$K_R = -\left(z_R + a_H(\varepsilon^*, \beta)z_H(\beta)\right)F_Y \quad (58)$$

$$M_R = z_{HX}(\beta)F_X \quad (59)$$

$$N_R = \left(x_R + a_H(\varepsilon^*, \beta)x_H(\beta)\right)F_Y \quad (60)$$

The longitudinal rudder force can be directly transferred to the ship's longitudinal force. The heave does not seem to be affected by the rudder, but the sway force and the moments depend on the rudder forces and the extra asymmetries induced by the hull. Figure 10 shows values of the different correlation coefficients in the first quadrant. The a_H parameter increases with decreasing under keel clearance, but at the same time the application points x_H and z_H move towards zero.

7 VALIDATION

7.1 CAPTIVE

Figure 11a, presented in Appendix 1, shows the correlation between the measured and modelled forces, moments or positions in every degree of freedom for 20% ukc. The correlation coefficient is always more than 90%, the trim being the most difficult degree of freedom to model.

Some captive runs were not used to determine the model coefficients, but to check the prediction capabilities of the simulation model in a rather complex trajectory. Two examples are shown in Figures 11b and 11c. In validation test 1 the longitudinal ship speed was constant and equal to 0.125 m/s (2.1 knots at full scale), while the rudder was harmonically varied between ± 35 deg. In validation test 2 the rudder was also varied harmonically between ± 35 deg and the longitudinal speed between 0 and 0.25 m/s (4.2 knots at full scale). The other kinematic and control parameters were varied according to the bottom graphs of Figure 11b and 11c.

Overall, the longitudinal force, sway force and yawing moment are accurately predicted. In the other degrees of freedom the predictions are fair enough for their intended purpose. The mean sinkage for instance has some underestimation, but was very small during the validation tests.

7.2 FREE RUNNING

In Figure 12 (see Appendix 2) all SIMMAN 2014 free running manoeuvres at 20% ukc are compared with the simulation prediction. In every graph the SIMMAN results are presented with grey curves. A black line is the prediction of the 6 DOF model presented in this article. In some graphs a dashed line is present, which is the prediction of the model presented in [3,4]. A coloured line is a prediction with modifications to the 6 DOF model, see section 8. Both the simulations and the free running results were scaled to full scale by means of Froude scaling only.

The 6 DOF manoeuvring model is better at predicting the trajectories than the model based on a limited number of tests. This was already suggested in [3] and illustrated in [4] based on the shortcomings of a 4 DOF model derived from only 97 captive model tests. Nevertheless, the 6 DOF manoeuvring model seems to underestimate the overshoot angles during the zigzag tests with larger discrepancies for the 10/2.5 zigzag tests. This underestimation was not only the case for the previous mathematical model described in [3] but is also observed for other ship models in very shallow water. As was concluded in [4] both empirical and PMM based mathematical models predict a more course stable KVLCC2 in 20% UKC. The global speed evolution during the manoeuvres seems well predicted, but both the drift angle and the yaw rate should be larger.

The largest deviations are seen for the roll angle (only shown for the partial turns). However, the roll angle during the free running tests is always towards starboard side, which suggests that the measurement in the free running tests is probably biased. In general the sinkage and trim of the vessel are reasonably well predicted, with a small underestimation for the sinkage.

8 SENSITIVITY ANALYSIS

In order to predict the SIMMAN 2014 free running manoeuvres in an accurate way, some coefficients of the mathematical model can be tuned. In theory any coefficient could be tuned and many possibilities exist to reach the same trajectory. In this case the period of the zigzag manoeuvres and the turning circle radius seems correctly predicted, which means that rudder forces and the yawing moment are adequately predicted.

The lower overshoots and corresponding low rate of turn and drift angle mean an unbalance, which can also be observed in the so-called pivot point (defined by $-v/r$, shown in Figure 13) which is the longitudinal position on the ship that is not subjected to lateral movement referred to the ship's trajectory. In a zigzag manoeuvre this pivot point shifts with every rudder reversal, but in the simulations the shift occurs too fast (low overshoot). In addition, the average position seems to be closer to midships compared to the free running trials. The shift towards midships is a typical phenomenon in shallow water, which was already observed for captive model tests in [8], but perhaps this does not happen during free running trials in very shallow water which are more scarcely available.

The position of the pivot point can be influenced by decreasing $Y'^{(\beta)}$, $Y'^{(\gamma)}$ or $Y'^{(\dot{x})}$ rather significantly, which was performed here for the 20/5 zigzag tests. The results are represented by the coloured curves in Figures 12 and 13. This way the simulations and the free running results are in agreement for the 20/5 zigzag tests. Further tuning would be needed for the 10/2.5 zigzag tests. Yet, it does not explain why in the captive tests a larger sway force in drift and/or yaw is measured than what can be expected during free running tests. More research is needed, for instance on the influence of the turning point during captive harmonic yaw tests. As already mentioned in [4] flow measurements in captive and free-running tests could help in understanding the steady or transient behaviour of the water flow in the tank. These flows could further be compared with flow predictions from RANS calculations using CFD techniques so that the specific hydrodynamics in shallow water are better understood.

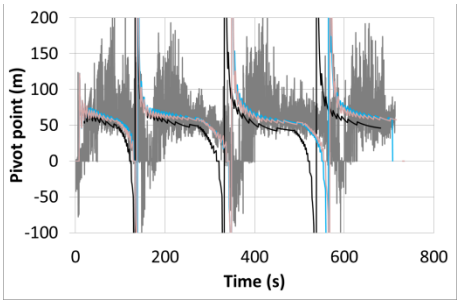

Figure 13. Evolution of pivot point during 20/5 zigzag test, starting to portside.

9 CONCLUSIONS

In this article the 6 DOF mathematical manoeuvring model is introduced, presently in use at FHR. The main input for this mathematical model is based on captive model tests, where the ship's motion is forced in the 3 horizontal degrees of freedom, while the ship's roll angle is fixed (and kept at 0 deg) and the heave and pitch motions are free. To use such test results, some assumptions are needed and sometimes numerical input is needed to assess the ship's response in the vertical degrees of freedom.

The predictions of the mathematical model for the KVLCC2 have been compared with the outcome of the SIMMAN 2014 free running tests at 20% ukc. The agreement is acceptable, except for the underprediction of the drift and yaw rate. This phenomenon has been observed for other ship models at very low under keel clearance and will receive more attention in future research.

10 REFERENCES

1. Delefortrie, G.; Vantorre, M.; Eloot, K. (2005). Modelling navigation in muddy areas through captive model tests. *J. Mar. Sci. Technol.* 10(4): pp. 188-202. dx.doi.org/10.1007/s00773-005-0210-5.

2. Delefortrie, G.; Geerts, S.; Vantorre, M. (2016). The Towing Tank for Manoeuvres in Shallow Water. *MASHCON 2016*, Hamburg, Germany.

3. Delefortrie, G.; Eloot, K. (2014). Mathematical Model for Shallow Water Manoeuvres with the KVLCC2 as used in SIMMAN 2014. *Preprints of SIMMAN 2014*, Lyngby, Denmark.

4. Eloot, K.; Delefortrie, G.; Vantorre, M.; Quadvlieg, F. (2015). Validation of Ship Manoeuvring in Shallow Water through Free Running Tests. *OMAE 2015-41912*, St. John's, Canada.

5. Tuck, E.O. (1966). Shallow-water flows past slender bodies. *J. Fluid Mech.* 26: pp. 81–95

6. www.SIMMAN2014.dk

7. Lataire, E.; Vantorre, M.; Delefortrie, G. (2012). A prediction method for squat in restricted and unrestricted rectangular fairways. *Ocean Engineering* 55: pp. 71-80. dx.doi.org/10.1016/j.oceaneng.2012.07.009

8. Vantorre, M.; Delefortrie, G.; Laforce, E.; De Vlieger, H.; Claeys, S. (2003) Ship manoeuvring at very small and negative under keel clearance, *MCMC 2003*, pp. 55-60.

11 AUTHORS' BIOGRAPHIES

Guillaume Delefortrie, naval architect, is expert nautical research at Flanders Hydraulics Research. He is in charge of the research in the Towing Tank for Manoeuvres in Shallow Water, development of mathematical models based on model tests and is secretary of the 27th and 28th ITTC Manoeuvring Committee.

Katrien Eloot, naval architect, is senior expert nautical research at Flanders Hydraulics Research and guest professor at Ghent University. She is involved in research concerning ship hydrodynamics in shallow and confined water through experimental fluid dynamics and ship manoeuvring simulation. She is member of the PIANC Working Group 141 for Design Guidelines for Inland Waterways and working groups of the NATO Science and Technology Organisation.

Evert Lataire, naval architect, is currently assistant at the division of Maritime Technology at Ghent University. He has written a PhD on the topic of bank effects mainly based upon model tests carried out in the shallow water towing tank of FHR. His ten year experience includes research on ship manoeuvring in shallow and confined water such as ship-ship interaction, ship-bottom interaction and ship-bank interaction.

Wim Van Hoydonck, aerospace engineer, is nautical researcher at Flanders Hydraulics Research. He is involved in research concerning ship hydrodynamics and hydraulic constructions using Computational Fluid Dynamics (CFD). He is a member of working groups of the NATO Science and Technology Organisation.

Marc Vantorre, naval architect, is full senior professor of marine hydrodynamics and head of the Maritime Technology Division at Ghent University, Belgium. His research focuses on ship behaviour in shallow and confined waters, mainly in close co-operation with Flanders Hydraulics Research in Antwerp. He is former member of several PIANC Working Groups and former member and secretary of the ITTC Manoeuvring Committee.

Appendix 1. Comparison between measured and modelled forces at 20% ukc. Captive validation tests.

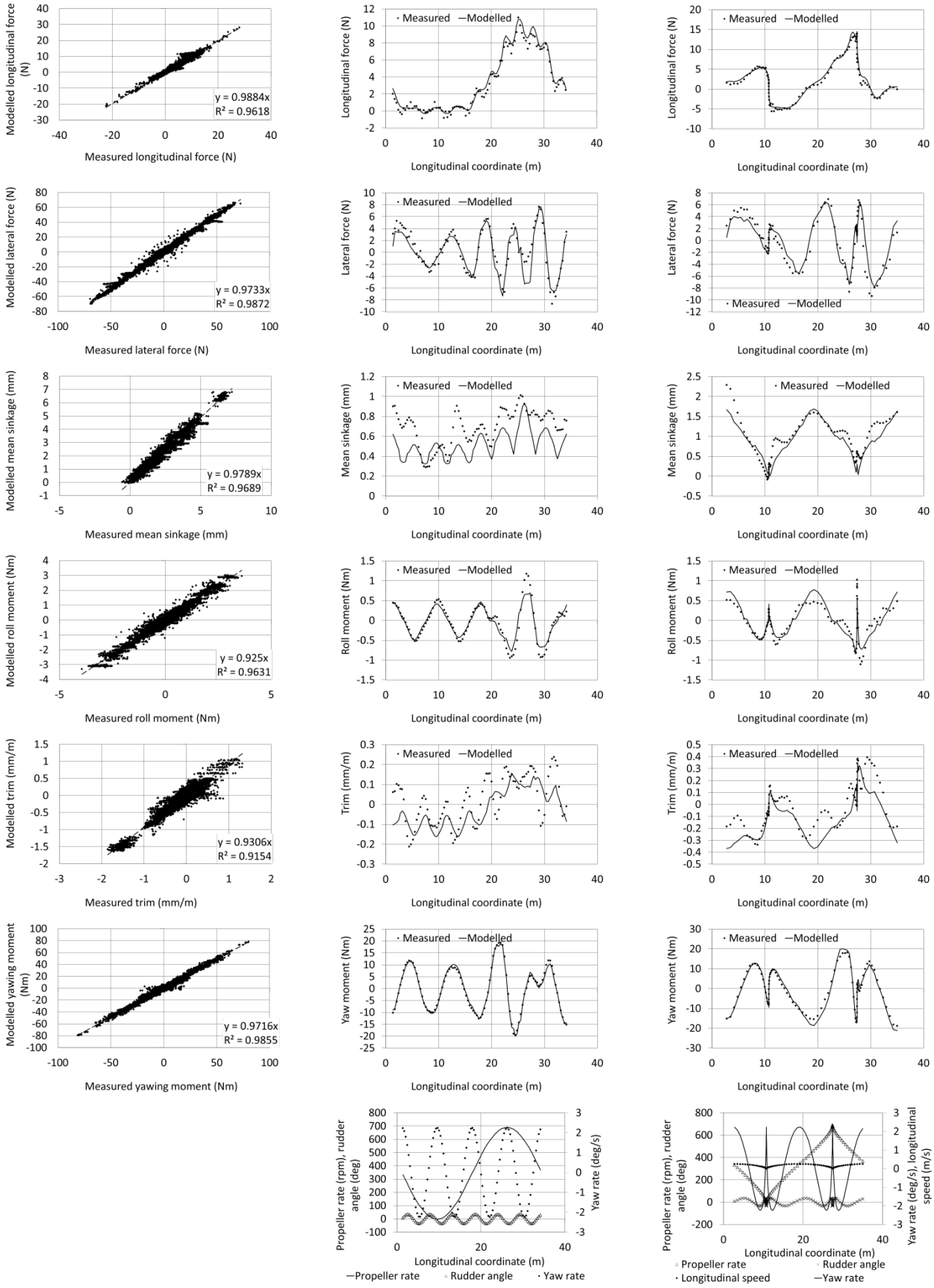

a) All tests b) Validation test 1 c) Validation test 2

Figure 11. Comparison between the measured and modelled forces and moments in captive model tests at 20% ukc.

Appendix 2. Comparison manoeuvring model with SIMMAN 2014 free running model tests

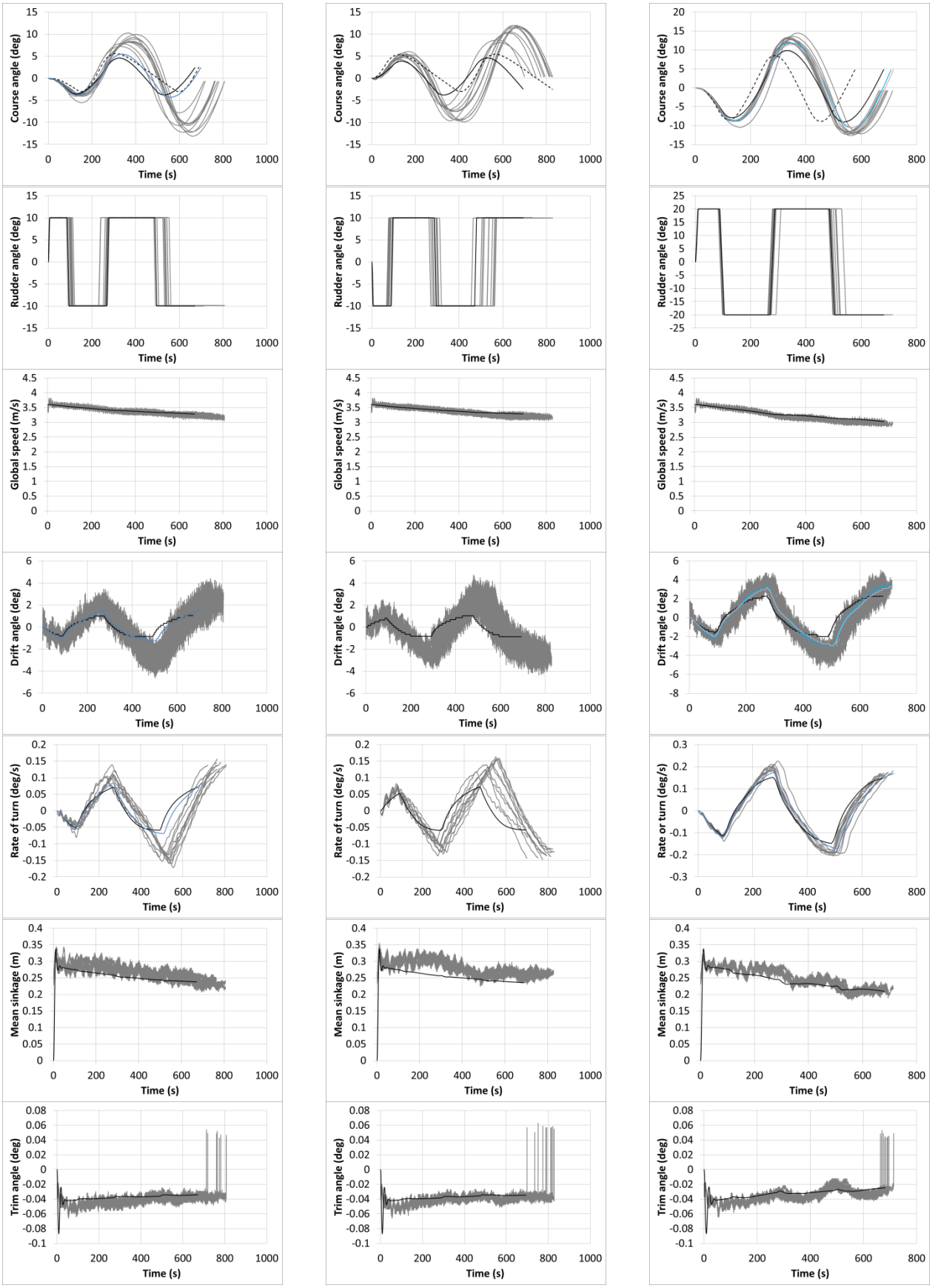

a) 10/2.5 zigzag test, starting to portside

b) 10/2.5 zigzag test, starting to starboard side

c) 20/5 zigzag test, starting to portside

{continues on next page}

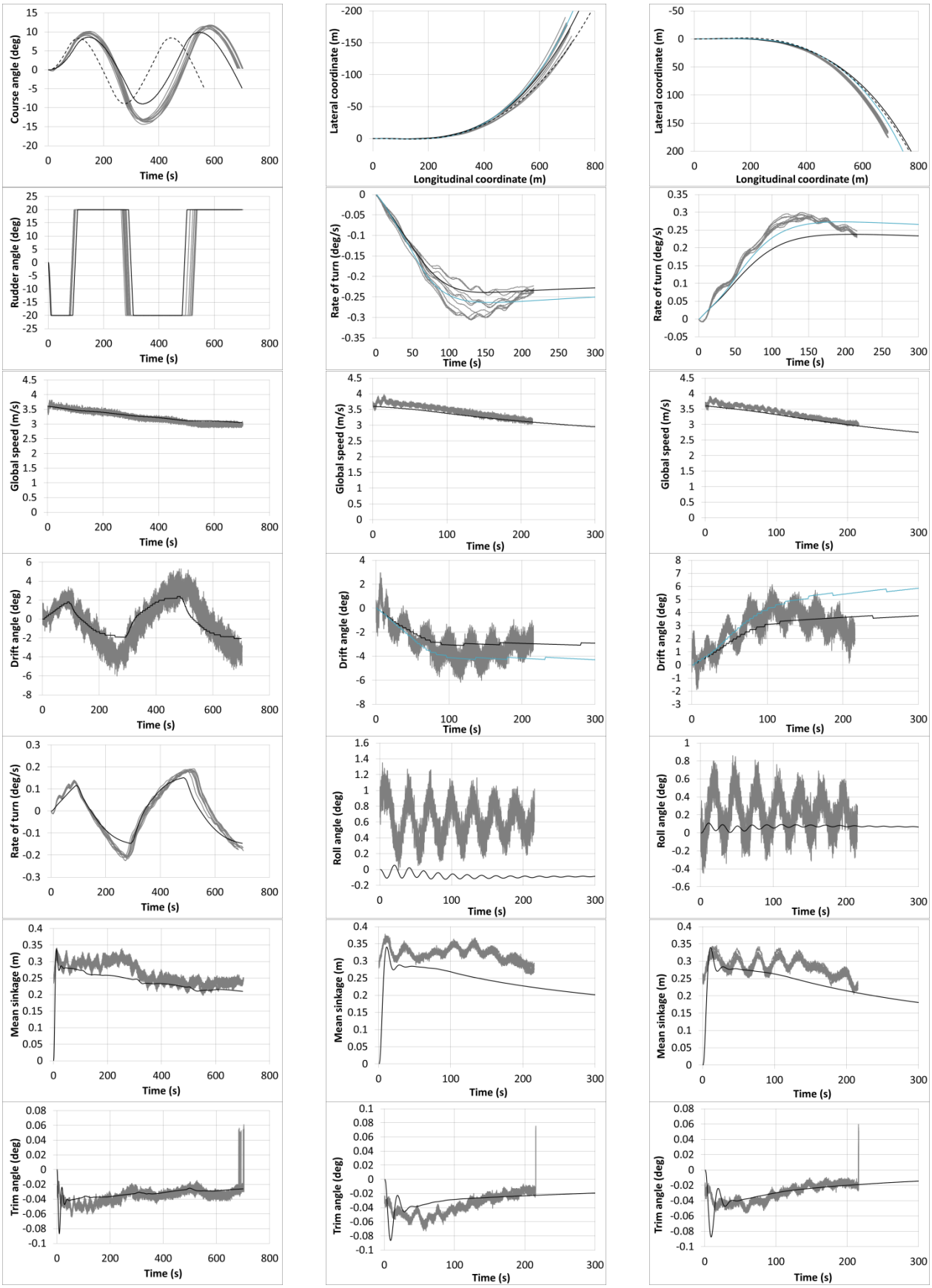

d) 20/5 zigzag test, starting to starboardside

e) 35 deg turn to portside

f) 35 deg turn to starboardside

Figure 12. Comparison between the SIMMAN 2014 model tests and the simulated manoeuvres (in prototype).